International Journal of Emerging Engineering and Technology (IJEET)
ISSN (e): 2958-3764
Volume: 3, Number: 1, Pages: 1 - 12, Year: 2024

Numerical Simulation and Parametric Investigation of Incremental Sheet Forming Process for Multilayer Sandwich Panels

Abdul Hameed Khan[1]*, Nasir Hayat[2], Hazrat Bilal[3]

[1]Department of Mechanical Engineering, University of Engineering and Technology, Mardan, Khyber-Pakhtunkhwa, Pakistan
[2]Department of Mechanical Engineering, University of Engineering and Technology, Lahore, Punjab, Pakistan
[3]Department of Civil Engineering, University of Engineering and Technology, Mardan, Khyber-Pakhtunkhwa, Pakistan
*Corresponding author: Abdul Hameed Khan (Email: engrabdulhameed@uetmardan.edu.pk)

***Abstract*- The multifunctional structure, i.e., multilayer sandwich panel (MLSP), exhibits properties like high rigidity, good specific strength, and lightweight and thermal resistance. Structural performance is attributed to these properties, making MLSP very favourable for producing highly reliable structures and increasing fuel efficiency due to its lightweight structure. Forming MLSP through conventional forming techniques such as deep drawing and punching is very challenging because it not only limits the formability but also requires special tooling and produces other undesirable effects. This work researched the feasibility of MLSP's formation through the single-point incremental sheet forming (SPIF) process. The SPIF process was modelled in the LS-DYNA to form MLSP into a benchmark shape. A tensile test was performed to evaluate the mechanical properties of the AL-1050. In the simulation, six more cases were also evaluated to see the effects of tool diameter, feed rate, and step size on the forming forces, formability, maximum percent thinning, etc. CATIA software generated the numerical code (NC) for the constant Z-level tool path and fed it to the CNC machine to perform the SPIF experiment on the MLSP. The larger tool diameter contributed to smaller forming forces, good formability, and less fracture area. The crack area and wrinkling tendency increase with the increase in feed rate first and then decrease with a further increase in feed rate. There was good agreement between the simulated and experimental formed geometrical shapes, proving that SPIF is feasible for forming multilayer sandwich structures.**

***Index Terms*- forming limit diagram, formability, multilayer sandwich panel, single point incremental forming.**

I. INTRODUCTION

A. Background

Many industries, such as transportation, defence, architecture, and aviation, must find effective solutions to improve fuel efficiency through structural design and innovations. Structures in the mentioned industries are considered to have excellent performance with good rigidity, specific strength, high thermal resistance, vibration dampening effect, good shock absorbing capacity, and be lightweight.

To meet these structural requirements, the most suitable structures are composite structures, but their application is limited due to the high cost of processing. A multilayer sandwich panel (MLSP) consists of two or more layers of sheets, usually two, made of one plane sheet and one dimple sheet bonded together with appropriate bonding. MLSP provides a cost-effective and lightweight solution without losing structural performance. The conventional forming processes mostly form unilayer structures. However, various flaws have been observed when the conventional forming methods are used to create the MLSP structures, which are non-uniform thickness distribution, limited formability, high forming forces, loss of structural integrity, and higher cost of special tooling and configurations, etc.

Single point incremental sheet metal forming (SPIF) is a forming technology that can effectively form MLSP. The process of ISF was patented in 1967 by Matsubara. It involved the deformation tool, metal sheet, blank holder, and backing sheet. The tool is clamped to the CNC chuck, which is driven in the tool path according to the required geometry. The blank holder holds the worksheet into place when the forming tool deforms the sheet. SPIF process involves many geometrical, material, and process parameters that determine the final product quality. The formability of the sheets greatly depends on these parameters. The schematic diagram of SPIF shows most of these parameters, along with the tools and materials required, as shown in Fig. 1.

For incremental sheet forming, a rigid hemispherical tool is usually used. The diameter of the tool influences the formability and surface roughness, and typical diameters taken are in a range of 6 to 20 mm [1].

There are important geometric parameters involved in the SPIF, as shown in Fig. 1. Where h, t_0 , α , t_f ,ΔZ, and Δy represent the forming depth, initial blank thickness, wall angle, final sheet thickness, step size, and horizontal step size respectively. Apart from it the rotation speed (rpm), the feed rate (mm/min), friction condition, etc., significantly influence the formability and quality of the resulting part. Two important tool path strategies are constant Z-level and helical tool paths.

In a constant Z-level tool path strategy, the tool is moved over the surface in a completely closed shape in the plane, and only downwards and instantaneous plunge motion is created at

one step. In the helical path, the tool is constantly given downward motion as it is moved along the way.

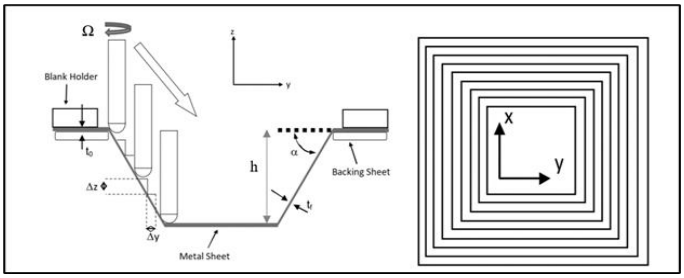

Fig.1. Showing the basic incremental sheet forming process: tools, process parameters and material

Each tool path strategy has its advantages [2, 3]. In some cases, constant Z-level strategy outperforms, while helical paths give better results in other cases.

The process & geometric parameters were thoroughly analyzed to increase the sheet's formability [4]. Forming limit diagrams are usually drawn to show the strains that can be imparted to the sheet in a safe-to-form area. The thickness distribution remains uniform when the material is unstretched or undeformed. Still, when the sheet is deformed to high depths, the thickness distribution of the sheet drastically changes to non-uniform. Non-uniform thickness distribution results in the thinning of the sheet material and produces stress concentration, and reduces the strength.

The feasibility of incremental sheet forming for the forming of a sandwich structure was assessed for the structures consisting of four types of sandwiches i.e., Mild Steel/Polypropylene/Mild steel, Aluminum/Polypropylene/Al, Stainless steel /SS fibre/ Stainless steel, and Al/Al foam/Al. These four samples of sandwich structures were evaluated for their formability, and their different failure modes were investigated. It was revealed that sandwiches with incompressible and ductile cores could be deformed through incremental sheet forming [5]. Curved panels made of the egg-box core were investigated for the feasibility of the multi-point incremental sheet forming and the failure modes of the skin sheet, which were wrinkling, dimpling of the skin sheet, and core fracture.

An analytical model for the skin sheet wrinkling, dimpling, and limiting radius of bending for wrinkling was also determined in terms of the material and geometric properties of the sandwich plates [6]. Experimental and numerical studies for the measurement of the formability of sandwich plates with trapezoidal cores (bidirected) through multi-point incremental sheet forming were conducted and determined that formability depends on the geometric parameters: formability of smaller thickness of the sandwich skin with a small size core is limited by the buckling, and that of thicker skin size and the heightened core is limited by skin wrinkling and dimpling [7].

The forming limit diagram of AA5052/polyethylene/AA5052 was drawn, which implies that such sandwiches have better formability than single-layer AA5052 sheets and links the formability to the thickness of the polyethylene core in a sandwich [8]. Characterization of steel/polymer/steel multi-layer sandwich was carried out. It showed that the faceplate and core's thickness significantly affect the thinning behaviour in deep forming, and the increase in core thickness contributes to cracking [9]. Numerous other researchers worked on the forming, thermoplastic behaviour and failure analysis, and modes of failure of polymer core-based sandwiches and found that the polymer bonding is limited, and polymer materials are not weldable; thus, sandwiches of polymer cores are not used in the automotive industry [10-15].

The performance of honeycomb sandwiches through bending and in-plane compression tests was assessed, and experimental results for the crash behaviour and the detailed collapse mechanisms were obtained and reproduced by numerical methods [16]. The experimental and numerical studies were performed to evaluate the sandwich's transverse shear modulus, which was made by stamping a dimple-shaped core and brazing it to the face sheet. The four-point bending test was performed to reveal the dimple sheet's bending behaviour and found that the small dimple width-to-height ratio and large bonding land-to-dimple width ratio contribute to the highest transverse shear modulus [17].

The energy absorption capacity of a sandwich, i.e., a sandwich from an aluminum face sheet and a metal hexagonal honeycomb as the core, was investigated, and it reported that the specific energy absorption is increased by increasing the thickness of the honeycomb core, decreased if the wall thickness of the honeycomb is increased. This parameter has no dependence on the face sheet thickness [18]. The energy-absorbing characteristics of the sandwich panels whose core is made of one spherical face end and the flat end face were studied and informed that by increasing the wall thickness of the core wall, the energy absorbing capacity is increased, with the spherical face part more predominantly than the flat face and declared these characteristics of such cores are greater than egg-box and other metallic cores [19].

Mathematical relationships of sheet thickness, wall angle, tool diameter, and step size of AA3003 sheet material with force components in three directions were constructed. To formulate force relationships with process parameters, truncated cones were formed by the incremental sheet-forming method [20]. Adaptive mesh technique in LS-Dyna explicit was utilized for creating process having localized deformations to drastically reduce forming simulation time by 50% without compromising the results [21].

The main objective of the current research is to simulate the single-point incremental sheet forming (SPIF) process for the multilayer panels and to validate the formed geometry experimentally and forming limit curves. The other objectives are the assessment of the formability of the multilayer structure in the SPIF `process through truncated rectangular pyramid benchmark shape, visualization of the forming evolution of sheets in the multilayer structure, determination of the influence of the feed rate, step size, and tool diameter on the forming forces of the sandwich sheet analyzing the thickness

distribution in the multilayer sandwich sheet, evaluation of the stress and strains present in the sandwich structure and to examine the different failure modes of the dimple sheet during incremental forming of the sheet.

This paper is structured so that the methodology is described in full in Section II, along with the AL-1050 material parameters, the SPIF process setup, and the LS-DYNA simulation model. Section III presents the tensile test results for AL-1050 and the effects of various process parameters (tool diameter, feed rate, step size) on forming forces and formability. Comparing the simulated and experimental geometries and examining the forming limit curves, Section III also covers the experimental validation of the SPIF process. The failure modes seen throughout the forming process are covered in this section, which offers insights into wrinkling tendencies and crack formation. Section IV summarizes the main conclusions and offers recommendations for further research.

B. Motivation and Contribution

The following are the novelty and main contributions of the current study:

1. This study uses a comprehensive approach to exploring the feasibility and optimization of SPIF for MLSP, an area that has yet to be extensively researched.
2. The combination of simulation, experimental validation, parameter analysis, and failure mode investigation provides a robust framework for future studies and industrial applications.
3. Research on using SPIF on MLSP needs to be more noticed. Although SPIF was designed for single-layer sheet metals, more is needed to know how well it works and how to optimize it for MLSP. Alternative procedures are necessary since traditional MLSP forming methods frequently result in problems, including uneven thickness distribution and high forming forces.
4. Numerical simulations and experimental validations need to be better integrated to assess the formability and mechanical properties of MLSP under SPIF.
5. This research facilitates the effective production of lightweight, high-performance MLSP structures.

II. METHODOLOGY

The process flow diagram shown in Fig. 2 depicts the step-by-step approach to this research. This diagram describes the material, CAD modelling, simulation, fabrication of the MLSP, and the SPIF experiment of the research.

A. Materials and CAD Modelling

The plane sheet was created with a thickness of 2.5 mm, and the length and width are equal to 270mm and 250 mm, respectively, as shown in Fig. 3 (B). The height of the dimple was selected as 6 mm, and the full model is shown in Fig.3 (C). These three parts were assembled using assembly options and tools. The assembly of the dimple sandwich has been shown in Fig. 3 (D). This model was used for subsequent simulation.

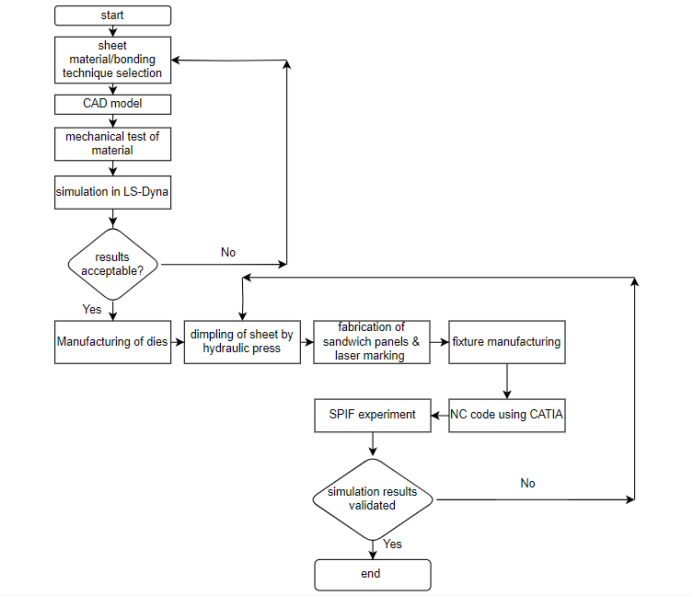

Fig.2. Flow chart for methodology

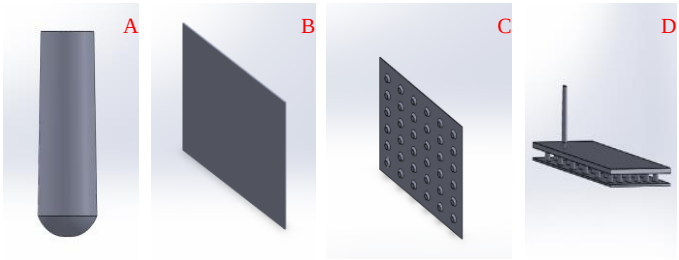

Fig.3. Modelling in Solidworks; (A) 3D model of tool, (B) Plane sheet model, (C) model of dimple sheet, (D) Assembly of sandwich panel

B. Mechanical Test for Material Properties

To simulate the SPIF in the LS-Dyna, the mechanical properties of sheet and tool materials must be evaluated and known, including the young modulus, Yield point, and poison ratio. The stress vs. strain curve of the tensile test for the sheet material AL1050 in the rolling and transverse directions of the sheet was achieved using the 2000KN, Ibertest, universal testing machine. For this purpose, the flat specimen was used with length, width, and thickness of 310 mm, 26mm, and 2.5 mm, respectively. Flat-type gripers were used to clamp the tensile test specimen firmly. This test was carried out according to the tensile test standard (ASTM E8/E8M) with a loading rate of 5.08 mm/min, shown in Fig.4. (A). The specimen under the test is shown in Fig. 4 (B), and the resulting stress vs. strain curve for the AL1050 in both rolling and transverse directions is shown in Fig. 4 (B). The material properties are listed in Table1.

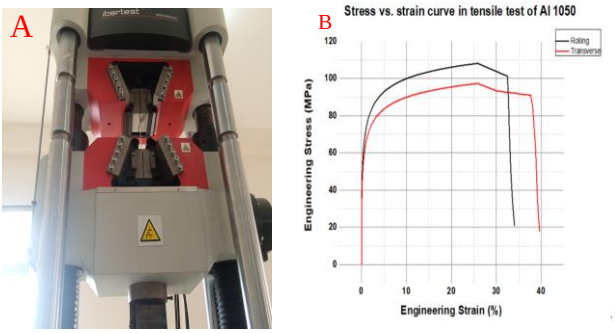

Fig.4. Tensile test; (a) AL1050 Specimen under the test, (b) Stress vs. strain curve for the Al 1050 specimen in rolling and transverse directions

TABLE I
MECHANICAL PROPERTIES OF AL 1050 MATERIAL

Young Modulus	Yield Point	Density	Poison ratio	% Elongation
(GPa)	(MPa)	(kg/m3)		%
68.95	69.3	2713	0.33	24

C. Numerical Simulation in LS-Dyna Software

The single-point incremental sheet forming of a panel with a dimple core was simulated in the LS-PrePost processor using its user interface. LS-Dyna is the most effective package for the finite element analysis of complex real-world problems in the manufacturing, aerospace, and automotive industries.

Different keywords were used in the simulation of this process.
*CONTACT_AUTOMATIC_SURFACE_TO_SURFACE was used to define the interaction between the different parts. First, contact was established between the plane sheet and the tool. Here, the plane sheet was taken as the master segment and the tool as the slave segment. The static coefficient of friction can be assumed as 0.20 and the dynamic coefficient of friction as 0.15 as per Szpunar [22]. The second contact was made between the plane sheet and dimple sheet.

*CONTACT_TIED_SURFACE_TO_SURFACE code was used to produce contact with dimple and plane sheets. *MAT keyword was used to define the material model and parameters for sheets and the tool. Material properties from the tensile test were used to model the elastic and plastic parts of material behavior. *MAT_POWER_LAW_PLASTICITY was used to define this material behavior. The power-law plasticity model can be represented in the following way.

$$\sigma = K * [\ln(1 + \epsilon_E)]^n \quad \ldots\ldots\ldots\ldots\ldots\ldots (1)$$

Where K is strength co-efficient, n is the hardening exponent and ϵ_E is engineering strain. The stress vs. strain curve and equation. 1 were compared to get the values of the K and n which turned out to be 125.280 MPa and 0.2504 respectively. The value of the n is calculated by taking the slope of the stress-strain curve in the plastic region as follows.

$$n = \frac{\ln(\sigma_2^p) - \ln(\sigma_1^p)}{\ln(\varepsilon_2^p) - \ln(\epsilon_1^p)} = 0.2504 \quad \ldots\ldots\ldots\ldots\ldots (2)$$

Also, Strain rate parameters and rate effects are ignored. *020-Rigid was used to define the rigid behavior of the tool. *DEFINE_CURVE was used to import the displacement curves from the (.CSV) file for the motion of the tool. The benchmark shape for forming simulation i.e truncated rectangular pyramid was used. The value assigned to rotational velocity was 500 rpm or 52.36 rad/s in this analysis.

*BOUNDARY_PRESCRIBED_MOTION_RIGID was used to define the tool's motion (displacement and rotation). In this case, the tool motion was stepwise described by the x, y, and z displacement vs. time curves, and the degree of freedom was defined subsequently in each step. For instance, the degree of freedom in the X-direction displacement was 1, which is applicable in the X-direction translation.

*CONSTRAINED_GLOBAL option was used to define the boundary conditions on the edges of the sheets. The sheet is clamped at the edges with the help of a fixture that constrains the sheet in translational and rotational directions. The fixed support of the fixture in the SPIF can be modelled as the constrained rotational and constrained translation with the help of the *CONSTRAINED_GLOBAL option. *

SECTION_SHELL was used to set the element type (2D shell) and thickness of each sheet. So solid sheets, as modeled in the CAD system, were converted to the 2D shell with a respective thickness of 2.5 mm and 1.5 mm for the plane and dimple sheet, respectively. Element formulation for the 2D shell element (ELFORM) was set to Belytschko-Tsay, the default element formulation option with Lagrangian, the 2D element type. *SECTION_SOLID option was used to inform the Ls-Dyna that Solid 3D elements are applied to the rigid and solid tool with fully integrated S/R solid intended for elements with poor aspect ratio, which is an accurate formulation. The Auto Mesh was generated on the sheets and the tool with an element size of 16.

The quality of the mesh was further improved using Element_Generation and Node_Edit options. The resulting mesh is shown in Fig. 5 (A), (B), and (C).

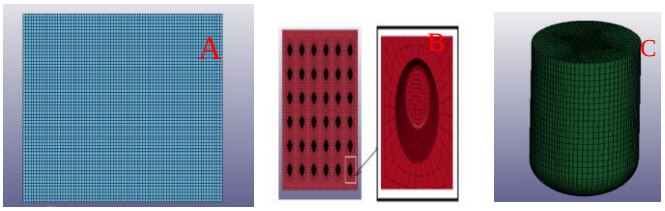

Fig.5. Showing the mesh; (A) Mesh on plane sheet, (B) Mesh on dimple sheet, (C) Mesh on deformation tool

The complete model consisted of 42578 elements in which there were 32418 shell elements and 10160 solid elements. The simulation was run on 4 processor computer which took about 12 hrs to compute the results. The structure was successfully deformed which is shown in Fig. 6. To study the effect of

different parameters like tool diameter, feed rate, and step size, 6 more models for the parameters shown in table 2 were simulated and their results are shown in the next section.

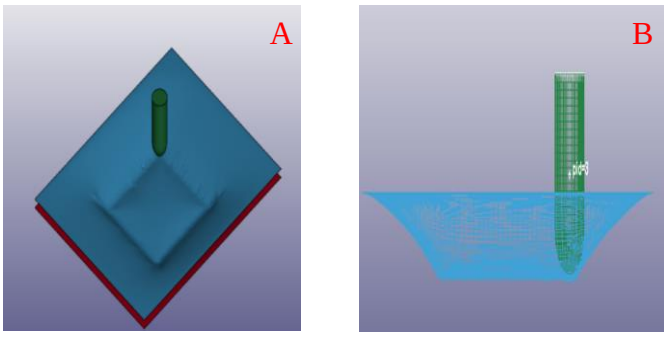

Fig.6. Deformed shape of the sandwich panel in FEA; (A) Isometric view, (B) Front view

TABLE II
DETAILS OF PARAMETERS FOR THE SEVEN SIMULATION RUNS

Run #	Tool dia	Step size	Feed rate	Angular speed
	(mm)	(mm)	(mm/min)	(rpm)
1	11	0.3	1200	500
2	11	0.6	1200	500
3	11	1	1200	500
4	11	0.3	1800	500
5	11	0.3	2100	500
6	15	0.3	1200	500
7	20	0.3	1200	500

D. Fabrication of MLSP

To conduct the SPIF process on the dimple sheet structure, it was primarily fabricated. The multilayer sandwich consists of one plane sheet and a dimpled sheet. Aluminum 1050 material was used for the plane and dimple sheet of thickness 1.5 mm and 2.5 mm respectively. Initially, the plane and dimple sheet were cut from the roll of the sheet into dimensions of 300 mm, and 270 mm.

Two dies namely male and female dies were manufactured using a vertical CNC machining center of ENSHU (ES450 model) Japan. For female and male dies, billets with 35mm height and 30 mm widths were machined to the required dimensions. The depth of the female cavity was 6 mm, and fillets were at the corner area of a 2mm radius. In the male part, the punch diameter was 11.85 mm which will allow accommodating the sheet thickness as well as prevent the shearing of the sheet during pressing through a hydraulic press machine. The manufactured dies are shown in Fig. 7 (A). In the stamping, a hydraulic press having a total capacity of 25 tons was employed. The female die was held on the bottom and the male on the top side and the sheet is placed in between the male and female die. The entire sheet dimpling was achieved in 6 individual pressing steps. Initially, the sheets were pressed in the hydraulic press machine with a 270 mm side. The remaining dimpling was made by successively setting a 42 mm distance each time from the middle axis of dimples created in the step just held before. The dimpled sheet has been shown in Fig. 7 (B).

Fig.7. Dies manufactured and sheet dimpling; (A) Manufactured male and female dies, (B) Pressed dimple sheet by hydraulic press machine

To assess the formability of the sandwich sheet it needs proper kind of marking or griding. As the sheet is formed the shape of the grid will be modified and different strain measurement techniques i.e optical method, strain gauges and mechanical extensometers, and ultrasonics method to measure strain can be used to construct forming limit diagrams (FLD). In the present work, the single circle grids and laser marking technique were selected to mark the sheet and obtain the FLD once incremental sheet forming is done on the sandwich structure. For the marking of the sheet, the portable, 50-Watt, fiber laser marking machine was used which is shown in Fig. 8 (A). It has a 300mm *300 mm working area with deep marking capability. Other main features of the machine consist of laser wavelength, maximum marking depth, marking speed, and minimum line width which were 1064nm, 1mm, 7000mm/s, and 0.01 mm respectively. The sandwich sheet made was placed on the working table and 8mm diameter single circle grids were made on the sheet, as shown in Fig. 8 (B). The line width of 0.01mm and cutting depth of 0.003 mm were used in this marking which doesn't affect the surface roughness or the material properties.

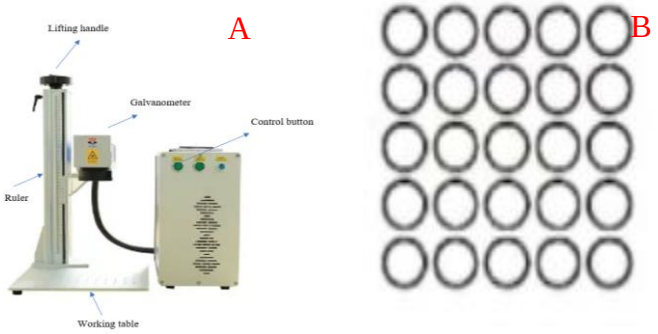

Fig.8. Laser Marking; (A) Laser marking machine, (B) single circle grids

The blank holder was needed for the accurate and tight clamping of the sandwich sheet during the incremental sheet forming. A fixture was fabricated for this purpose containing a backing plate, main vertical frame, and blank holding strips.

The height of the fixture was kept to 100 mm, and the length and width were 310 and 280 mm, respectively. For the backing plate, the central rectangular cut was made in the initial plate, and chamfers were made on the edges to prevent the sheet from cracking and other defects when it is formed. The main blank holder stand was held first, then the backing plate, sandwich sheet, and the blank holding strips were set over it, and bolts were tightened firmly.

After that, the 13 mm diameter cylindrical rod, made of carbon steel material, was chosen for a length of 100 mm. It was turned to 11mm diameter on the lathe machine, and a fillet of 5.5 mm radius was made through machining the cylindrical rod using lathe machine and the filleting tool. Finally, the surface finish of the tool was enhanced by grinding fine abrasion paper.

E. Experimentation of SPIF

Single-point experimental sheet forming was conducted on the sandwich sheet. The tool path, final product shape, and all the other parameters were decided and employed by generating numerical code (NC) through CATIA. This 3D model was created in the CATIA in the dimensions shown in Fig. 9 (A) and (B).

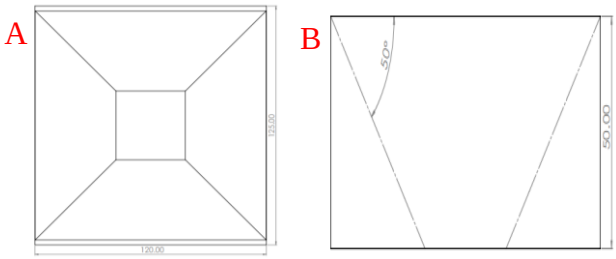

Fig.9. 3D model with dimensions for the NC code generation; (a) Top view of CAD model, (b) Side view of CAD model

In CATIA under processes in the process list tree, the part operation was added. In the resource list, three axes CNC machine was created and an endmill tool of 5.5 mm diameter was selected. From the main menu tool, option machining was activated and in the output option, the NC code extension was set to NC. The manufacturing process program option was utilized to open "generate NC code interactivity". In this window, the NC data type option was set to NC code, and it was executed. From the surface of the solid shape given in Fig. 9 (A) and (B), the NC code was generated. The values of process parameters that were used in the tool motion are given in table 3. Upon the successful creation of the NC code, it was fed to the CNC machine. The experiment on the forming of the MLSP through SPIF has been shown in Fig. 10 (A) and (B). To refer to a particular case the nomenclature used throughout this document includes the tool diameter, feed rate and the step size. For example, to refer to a case when the tool diameter is 11mm, feed rate is 1200 mm per minute and step size of 0.3 mm, the nomenclature will become 11mm1200mmpmin0.3mm.

III. RESULTS AND DISCUSSION

A. Forming Evolution of MLSP

As discussed in section II (C), seven simulations were performed to see the effects of different parameters on the resulting shape and how the material formed to achieve the final shape. The forming evolution for the percent forming cycle, i.e, 0%, 20%, 40%, 60%, 80% and 100% for the 11mm1200mmpmin case, is shown in Fig. 11 (A), (B) and (C).

The numerical forming evolution shows that the numerical code for the SPIF of the multilayer sheet was successfully created and thus proved correct. The numerical code can also successfully model the assumptions and different processes and geometrical parameters with great accuracy. Fig. 12 (A) and (B) show the experimental and simulated geometries after forming.

TABLE III
PROCESS PARAMETERS FOR THE TOOL PATH AND VELOCITY CREATION

S.No	Parameter	Unit	Symbol	Value
1	Feed rate	mm/min	f	1200
2	Plunge feed	mm/min	fp	100
3	Step depth	mm	h	0.3
4	Tolerance	mm	-	0.01
5	Spindle speed	rpm	Ω	500

B. Effect of Process Parameters on Forming Forces Parameters

To evaluate the effect of the process parameters like diameter of the tool, step size, and feed rate of the tool on the forming forces the reaction force on the tool in the Z-direction (direction perpendicular to the sheet) was calculated using the Ls-Dyna (bndout) option. The initial plot contained noisy data and suitable filters were applied to find the less noisy data.

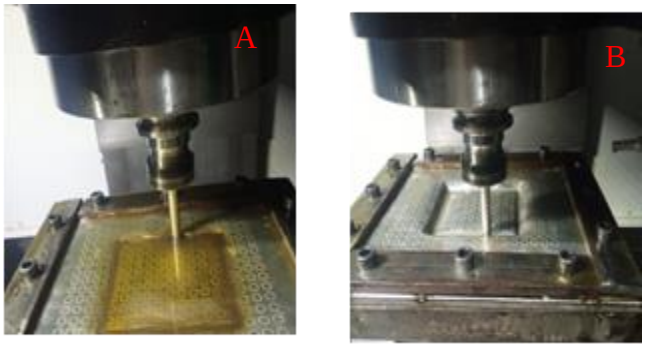

Fig.10. SPIF experiment in CNC milling machine; (A) At the end of half depth of tool, (B) At the end of full depth of tool

The filtered forming force vs. time graphs for simulation of 11mm1200mmpmin0.3mm case has been shown in Fig. 13. The effect of the tool diameter on the average forming force is shown in Fig. 14 (A). It is evident from the figure that the smaller tool requires high forming forces to deform the sheet

because with the smaller diameter tool the contact force is smaller, which results in less force being transferred to the sheet. Thus, more force needs to be applied to the tool. On the other hand, with a larger diameter tool, the contact surface is larger. Therefore, more force is transferred to the sheet and that's why the applied force on a tool is smaller.

Apart from it, the forming forces are reduced by increasing the step size in the Z-level tool path strategy which is shown in Fig. 14 (B). The effect of feed rate on forming forces is shown in Fig. 14 (C), the average forming forces are dependent on the feed rate. The forming forces remain high for the low feed rates and decrease for higher feed rates.

C. Formability and Forming Limit Diagram (FLD)

The formability of the sandwich sheet is measured numerically for all seven cases and experimentally for the (11mm1200mmpmin0.3mm). There are several ways in which the material can fail or tend to fail. These are cracks, risk of cracks, severe thinning, and wrinkling. From the numerical results of the mentioned case, it was apparent that there were a small number of cracks, especially at the corner of the plane sheet, and a few areas of wrinkling and severe thinning as shown in Fig 15 (A).

In addition to it, there was wrinkling in dimples, specifically in those areas where bending occurs to form the desired wall angle, as shown in Fig. 15 (B). Likewise, the different forming minor defect on the bonding side of the plane sheet is shown in Fig. 15 (C). The FLD for the 11mm1200mm/min0.3mm case is shown in figure 18. In this case, there was 0.1574% of the total sheet area subjected to cracks, 0.127% with severe thinning, and 3.08 % area with wrinkles.

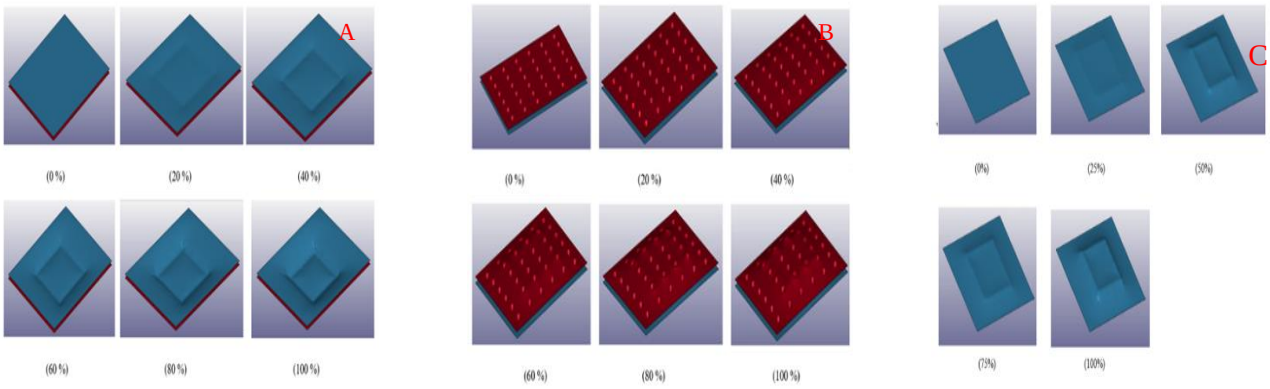

Fig.11. Numerical forming evolution; (A) For the plane sheet, (B) For the dimple sheet (C) For the plane sheet at bonding surface

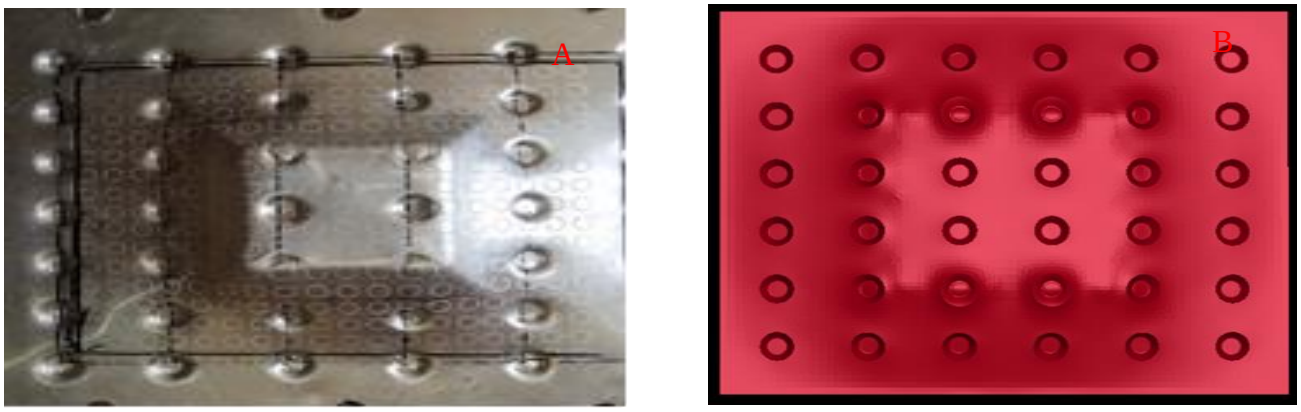

Fig.12. Formed geometries; (A) Experimentally formed geometry, (B) Simulated formed geometry

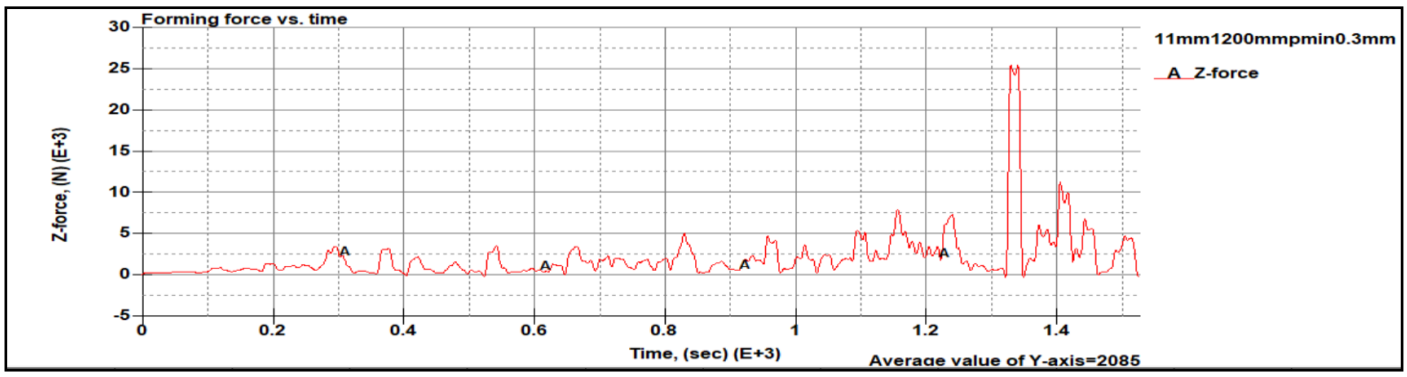

Fig.13. Forming force vs time graph for 11mm1200mmpmin0.3mm

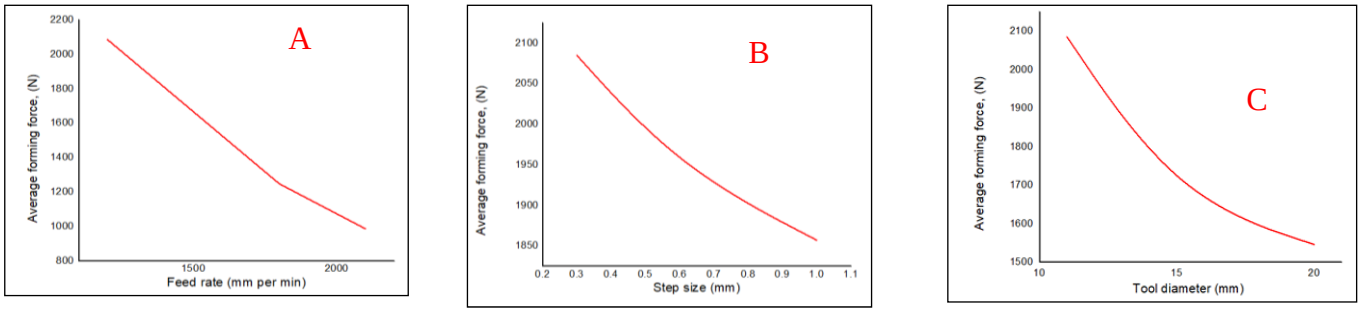

Fig.14. Effect of process parameters on the forming forces; (A) Effect of the tool diameter on the forming force, (B) Effect of step size on the forming force, (C) Effect of feed rate on the average forming force

The experimental FLDs were constructed by noting the change in the marked circles near the cracks/necking in the sheet material. The circles are converted to ellipses with a major diameter d_1 of and a minor diameter of d_2 after deformation as shown in Fig. 17. The change is measured through a traveling microscope.

The percent of major and minor strains are calculated as follows,

$\in 1$=major strain=(d1-2R)/2R×100% ……(3)

$\in 2$=minor strain=(d2-2R)/2R×100% ……(4)

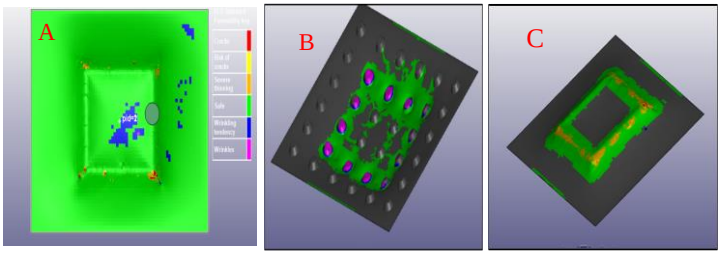

Fig.15. Forming defects; (A) Cracks, risk of crack, severe thinning, wrinkling tendency and wrinkles regions on the plane sheet, (B) wrinkling tendency and wrinkles region shown on the dimple sheet, (C) Different small failure regions on the bonding side of the plane sheet

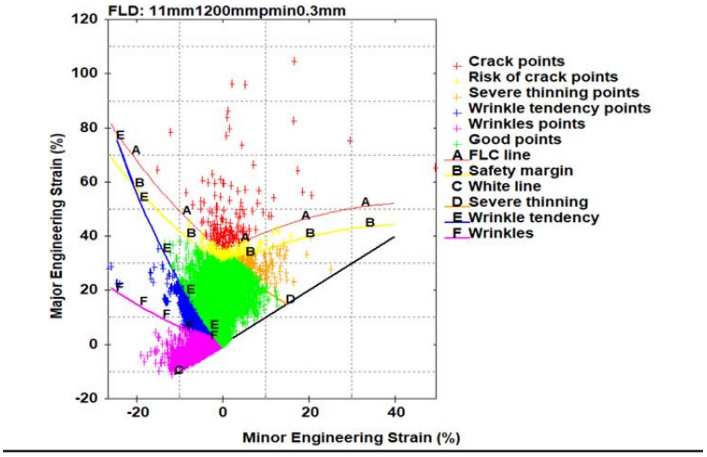

Fig.16. Forming limit diagram of 20mm1200mmpmin0.3mm case, calculated from the numerical results

The experimental FLD is shown in Fig. 18. The experimental and numerical FLDs showed a good correlation for a wide range of strains and the slight difference is due to the measured strains with a measurement uncertainty of 3-5%.

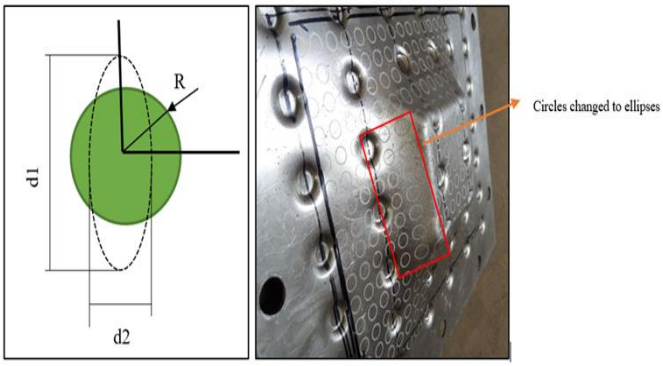

Fig.17. Showing the change of circle into ellipse; (A) Schematic showing the change of circles into ellipse, (B) resulting ellipses on the sandwich structure

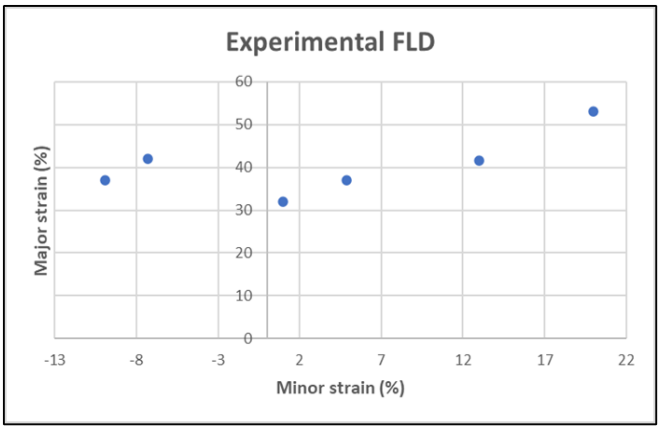

Fig.18: Forming limit diagram for the case 11mm1200mmpmin0.3mm calculated from experimental results

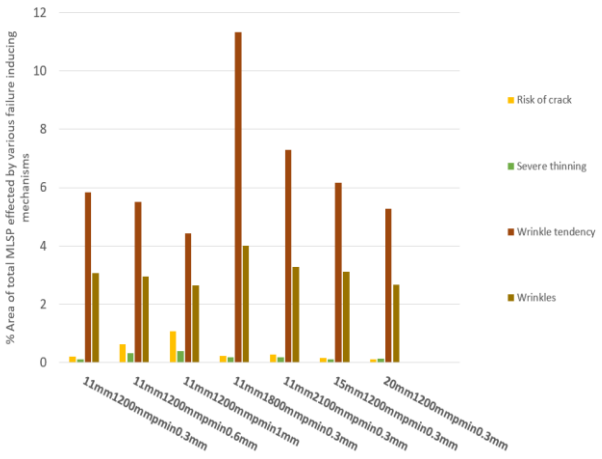

Fig. 19. Summary of formability of seven cases

A summary of the formability for seven cases is shown in Fig. 19, which is a chart showing the various failure-inducing mechanisms the sheets are vulnerable to. It shows for different cases the percentage area of the sandwich sheet affected by the failure mechanisms like cracks, risk of crack, severe thinning, wrinkling tendency, wrinkles, etc. it indicates that there are fewer cracks in the sandwich panel when the sheet is formed with larger diameter tool and larger cracks and less formability when the step size is increased. it also shows that the formability is greatly related to the feed rate of the tool and its formability is limited due to the feed rate which produces a high number of wrinkles.

D. Thickness distribution- percentage thickness reduction

The results for percentage thickness reduction for the plane sheet of the 11mm1200mm/min0.3 is shown in Fig. 20 (A). The thickness reduction for this case is very uniform and there is no such non-uniformity in the plane sheet of the MLSP during its SPIF forming. There are small locations for maximum thickness reduction (59.55%) near the rounds and most of the plane sheet is dominated by thickness reduction in the range of approximately 18 to 30 %. Similarly, percentage thickness reduction for dimple sheet is shown in Fig. 20 (B).

The maximum thickness reduction of 12% is found in the vicinity of the dimple grounds. These results indicate that the thickness distribution is very uniform and there are no peaks and troughs found in the sheet. It can be seen from the results that the percentage thickness reduction is directly related to the process parameter (step size) in the dimple sheet. For the plane sheet, the % thickness reduction first increases and then decreases with an increase in step size.

The thickness reduction increases drastically with an increase in feed rate for dimple sheets and for plane sheets the thickness distribution first increases and then goes on decreasing with an increase in feed rate. With the increase in tool diameter, the thickness reduction first increases and then starts decreasing for the dimple sheet, and for the plane sheet, percentage thickness reduction first decreases and then increases.

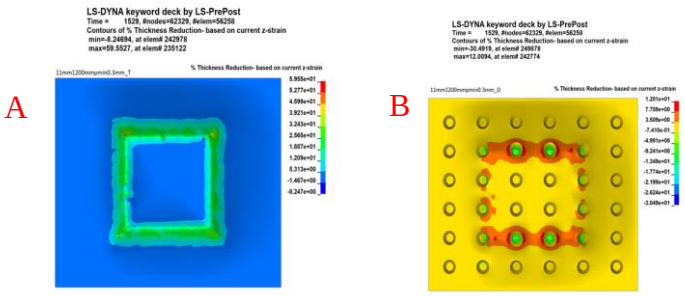

Fig.20. Percentage thickness reduction; (A) Percentage thickness distribution in plane sheet of 11mm1200mmpmin0.3mm, (B) Percentage thickness distribution in dimple sheet of 11mm1200mmpmin0.3mm

E. Stresses and Strains in the Formed MLSP

The stresses and strains remain in the sheet metal after the MLSP is formed; these stresses are called residual stresses. The residual stresses and strains are important factors determining how well-formed metal sheets perform in their service life and their behaviour to externally applied loads. The residual stresses and strains have been calculated in the current work, shown in Fig. 21 and Fig. 22, respectively, for the 11mm1200mm/min0.3mm case and discussed further in section I (D).

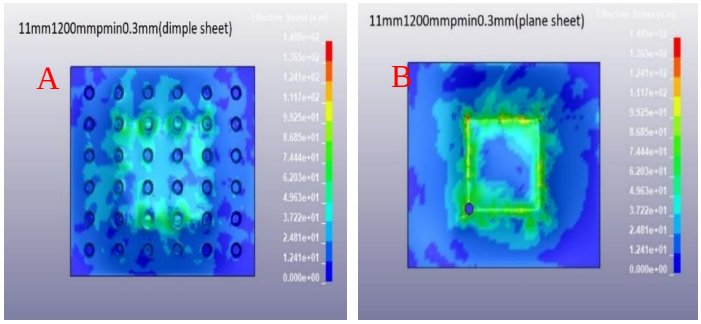

Fig.21. Stresses in formed MLSP of 11mm1200mmpmin0.3mm case; (A) Stresses in the dimple sheet, (B) Stresses in the plan sheet

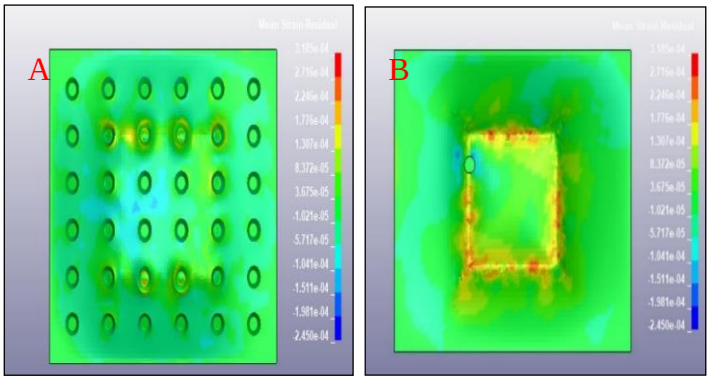

Fig.22. Strains in formed MLSP of 11mm1200mmpmin0.3mm case; (A) Strain in the dimple sheet, (B) Strain in the plan sheet

IV. CONCLUSIONS

In this research work, the finite element model was developed for the single-point incremental sheet forming process of multilayer sandwich panels. Later, the developed model was solved for seven sets of parameters to analyze the parametric simulations with help of the Ls-Dyna package. A tensile test was performed before performing simulations to calculate the mechanical properties of the AL-1050. The MLSP was developed through the male, and the female dies by pressing it with a hydraulic press, converting it to the dimple sheet, and bonding it to another sheet with help of epoxy resin. Several Ls-Dyna post-processing tools were used to assess the results and compare them. Results for the forming evolution, forming forces, FLDs, different failure mechanisms, thickness reduction, and stress and strains were derived. Finally, the following conclusion was obtained from the current work.

1. The SPIF is a feasible manufacturing process for forming MLSP.
2. When the combination of tool diameters and the feed rates were used in such a manner that large tool diameter i.e 20 mm and small feed rate i.e 1200 mm/min or small tool diameter i.e 11 mm and large feed rate i.e 2100 mm/min with constant step size of 0.3 mm, resulted in smaller sheet cracking areas of 0.063% and 0.070% respectively. Moreover, when the larger step size i.e 1 mm was used in forming of MLSP, resulted in 1.265% of the crack area. It indicates that for good forming smaller step sizes and the combinations of tool diameter and feed rate mentioned above should be used.
3. From results it is evident that the maximum percentage thickness reduction of 85.22% was achieved for the plane sheet at the condition of small tool diameter i.e 11 mm, small step size i.e 0.3 mm and feed rate of 1800 mm/min which is greater than the percentage thickness reduction of 37.34 % at 2100 mm/min feed rate condition. Such results suggest that the percentage thickness reduction depends strictly on the feed rates and there are optimum values of the feed rates that should be used to increase the percentage thickness reduction.
4. Tool diameters i.e 11 mm, 15mm and 20 mm result in 59.55%, 49.98%, and 55.98%
of thickness reductions respectively. Small tool diameters produce high thickness reductions but as the tool diameter is increased further beyond certain level this linear relationship doesn't follow. In view of above a generalized conclusion can be drawn as smaller tool diameter contributes to increased percentage thickness reduction.
5. Optimum values of the step size should be identified and used for the forming of MLSP as very small values or large values of the step size reduce the percentage thickness reduction of the sheet. Such conclusions were derived from the fact that the very small step size i.e 0.3 mm result in 59.55 %, very large step size i.e 1 mm result in 61.79% percentage thickness reduction while the optimum step size of 0.6 mm result in increased percentage reduction of 69.79%.
6. During the process of forming MLSP with the intermediate

feed rate of 1800 mm/min, the wrinkles were produced on 4.003% of the sheet and there were 3.08% and 3.28% wrinkled areas for the feed rates of 1200 mm/min and 2100 mm/min. Thus, it is concluded that the forming of MLSP should be performed at some intermediate values.

7. Also, the residual stress and strains are found to function of the process parameter.
8. It is concluded that the optimum process parameter must be selected before undertaking the process for increased formability, low forming forces, less residual stress and strains, and good percentage thickness distribution.

In the present work, the effect of only three parameters was analyzed (tool diameter, feed rate, and step size). However, there are other parameters such as type of sheet material, dimple sheet thickness, plane sheet thickness, bonding technique/material, dimple height, dimple bond land area, lubrication type, and spiral tool path. Apart from it, only a limited range of the three parameters was tested. The feed rate below 1200mm/min and above 2100mm/min, the tool diameter below 11mm and above 20mm, and step size below 0.3 mm and above 1mm can be also tested which may result in increased formability and minor thickness reduction. The above points are recommended for the future work of this research which can be investigated for improved results.

ACKNOWLEDGMENTS

Authors acknowledge the technical assistance provided by Pakistan Hunting and Sporting Arms Development Company, Peshawar and Ghulam Ishaq Khan Institute of Engineering Sciences and Technology, Topi, Pakistan in the use of CNC milling and hydraulic press machines respectively.

DECLARATION

a. Conflicts of interest – The authors declare no conflict of interest.
b. Availability of data and material – Not Applicable
c. Code availability – Not Applicable
d. Ethics approval – Not Applicable
e. Consent to participate – Written informed consent for publication was obtained from all participants.
f. Consent for publication – Written informed consent for publication was obtained from all participants.

REFERENCES

1. Kumar, A., Gulati, V., Kumar, P., Singh, V., Kumar, B., and Singh, H. (2019). Parametric effects on formability of AA2024-O aluminum alloy sheets in single point incremental forming," Journal of Materials Research and Technology, 8(1), pp. 1461-1469. DOI: https://doi.org/10.1016/j.jmrt.2018.11.001.
2. Said, L. B., Mars, J., Wali, M., and Dammak, F. (2016). Effects of the tool path strategies on incremental sheet metal forming process," Journal of Mechanics and Industry 17(4), p. 411. DOI: https://doi.org/10.1051/meca/2015094.
3. Yan, Z., Hassanin, H., El Sayed, M., Eldessouky, H., Djuansjah, J., Alsaleh, N., Essa, K., and Ahmadein, M.(2021). Multistage tool path optimisation of single-point incremental forming process," Materials, 14(22), p. 6794. DOI: https://doi.org/10.3390/ma14226794.
4. Kim, T., and Yang, D. (2000). Improvement of formability for the incremental sheet metal forming process," International Journal of Mechanical Sciences, 42(7), pp. 1271-1286.DOI: https://doi.org/10.1016/S0020-7403(99)00047-8.
5. Jackson, K., Allwood, J., and Landert, M. (2008). Incremental forming of sandwich panels," Journal of Materials Processing Technology 204(1), pp. 290-303.DOI: https://doi.org/10.1016/j.jmatprotec.2007.11.117.
6. Cai, Z., Zhang, X., and Liang, X. (2018). Multi-point forming of sandwich panels with egg-box-like cores and failure behaviors in forming process: analytical models, numerical and experimental investigations," Materials and Design ,160, pp. 1029-1041. DOI: https://doi.org/10.1016/j.matdes.2018.10.037.
7. Liang, X., Cai, Z., Zhang, X., and Gao, J. (2020). Plastic forming of the doubly curved surfaces of sandwich plates with bi-directionally trapezoidal cores of different sizes," Thin-Walled Structures,146, p. 106188. DOI: https://doi.org/10.1016/j.tws.2019.106188.
8. Liu, J., Liu, W., and Xue, W. (2013). Forming limit diagram prediction of AA5052/polyethylene/AA5052 sandwich sheets," Journal of Materials and Design, 46, pp. 112-120. DOI: https://doi.org/10.1016/j.matdes.2012.09.057.
9. Harhash, M., Carrado, A., and Palkowski, H. (2014). Forming limit diagram of steel/polymer/steel sandwich systems for the automotive industry," Advanced composites for aerospace, marine, and land applications, Springer, pp. 243-254.
10. Safaei, B., et al. (2019). Thermoelastic behavior of sandwich plates with porous polymeric core and CNT clusters/polymer nanocomposite layers. Composite Structures,**226**: p. 111209 DOI: https://doi.org/10.1016/j.compstruct.2019.111209.
11. Cui, Y., et al. (2019). Excellent energy storage density and efficiency in blend polymer-based composites by design of core-shell structured inorganic fibers and sandwich structured films. Composites Part B: Engineering, **177**: p. 107429 DOI: https://doi.org/10.1016/j.compositesb.2019.107429.
12. Harhash, M., Carrado, A., and Palkowski, H. (2014). Forming limit diagram of steel/polymer/steel sandwich systems for the automotive industry," Advanced composites for aerospace, marine, and land

applications, Springer, pp. 243-254. DOI: https://doi.org/10.1016/j.compstruct.2010.07.016.
13. Miller, W. (1980). Metal-Plastic laminates for vehicle weight reduction. SAE International: p. 481-490 DOI: https://www.jstor.org/stable/44632435.
14. Djama, K., et al. (2019). Mechanical behaviour of a sandwich panel composed of hybrid skins and novel glass fibre reinforced polymer truss core. Composite Structures, **215**: p. 35-48 DOI: https://doi.org/10.1016/j.compstruct.2019.02.033.
15. Mitra, N., et al. (2019). Interfacial delamination crack profile estimation in polymer foam-cored sandwich composites. Engineering Structures, **189**: p. 635-643 DOI: https://doi.org/10.1016/j.engstruct.2019.03.076.
16. Sun, G., Xintao, H., Chen, D., and Li, Q. (2017). "Experimental and numerical study on honeycomb sandwich panels under bending and in-panel compression," Materials and Design, 133.DOI: https://doi.org/10.1016/j.matdes.2017.07.057.
17. Besse, C., and Mohr, D. (2012). Optimization of the Effective Shear Properties of a Bidirectionally Corrugated Sandwich Core Structure," Journal of Applied Mechanics, 80(1). DOI: https://doi.org/10.1115/1.4006941.
18. Zarei Mahmoudabadi, M., and Sadighi, M. (2019). Experimental investigation on the energy absorption characteristics of honeycomb sandwich panels under quasi-static punch loading," Aerospace Science and Technology, 88, pp. 273-286. DOI: https://doi.org/10.1016/j.ast.2019.02.035.
19. Haldar, A., Zhou, J., and Guan, Z. (2016). Energy absorbing characteristics of the composite contoured-core sandwich panels," Materials Today Communications, 8, pp. 156-164. DOI: https://doi.org/10.1016/j.mtcomm.2016.08.002.
20. Aerens, R., Eyckens, P., Van Bael, A., and Duflou, J. (2009). Force prediction for single point incremental forming deduced from experimental and FEM observations," International Journal of Advanced Manufacturing Technology, 46, pp. 969-982. DOI: 10.1007/s00170-009-2160-2.
21. Suresh, K., and Regalla, S. (2014). Effect of Mesh Parameters in Finite Element Simulation of Single Point Incremental Sheet Forming Process," Procedia Materials Science, 6, pp. 376-382. DOI: 10.1016/j.mspro.2014.07.048
22. Szpunar, M., Trzepieciński, T., Żaba, K., Ostrowski, R., and Zwolak, M. (2021). Effect of Lubricant Type on the Friction Behaviours and Surface Topography in Metal Forming of Ti-6Al-4V Titanium Alloy Sheets," Journal of Materials ,14(13), p. 3721. DOI: https://doi.org/10.3390/ma14133721.